CrossMark

A high-sensitivity temperature sensor based on Sagnac interferometer employing photonic crystal fiber fully filled with ethanol

Min Shi[1] · Shuguang Li[1] · Hailiang Chen[1]

Abstract

A high-sensitivity temperature sensor based on photonic crystal fiber Sagnac interferometer is proposed and studied. All holes of the PCF are filled with ethanol with capillarity. The cladding air holes are uniform arrangements. The two air holes around the core are removed to form new core modes with high birefringence. The sensitivities of the temperature can be up to −8.7657 and 16.8142 nm/°C when temperature rises from 45 to 75 °C and the fiber length is 5.05 cm. And when temperature rises from 10 to 45 °C, the sensitivity can reach −7.848 and 16.655 nm/°C with fiber length 2.11 cm. The performance of the selective-filled and the fully-filled PCF with temperature from 45 to 75 °C and fiber length 5.05 cm are analyzed and compared. The fully filling can better achieve PCF's sensing performance. The simple structure and high sensitivities make the temperature sensor easy to achieve. The temperature sensor with high sensitivities and good linearity has great application value for environmental temperature detecting.

1 Introduction

Various photonic crystal fiber (PCF) [1]sensors have attracted extensive attention for its excellent performance, such as anti-interference ability and high precision. PCF temperature sensors show great advantages in medical, electric system, architecture and other fields, and have been widely used in various environmental engineering measurement. Geng et al. [2] proposed a temperature sensor based on fully liquid-filled PCF Mach–Zehnder interferometer. Two arms of the Mach–Zehnder interferometer are composed of core modes LP01 and LP11. The sensitivity is −1.83 nm/°C with the temperature increasing from 23.2 to 58.2 °C. Hameed et al. [3] studied a temperature sensor with PCF filled with liquid crystal and metallic nanorods. The coupling wavelength where the core guide mode couples with surface plasmon mode shifts with temperature. The

✉ Shuguang Li
shuguangli@ysu.edu.cn

Min Shi
18233565120@sina.cn

1   State Key Laboratory of Metastable Materials Science
     and Technology and Key Laboratory for Microstructural
     Material Physics of Hebei Province, School
     of Science, Yanshan University, Qinhuangdao 066004,
     People's Republic of China

sensitivity is 10 nm/°C with the temperature range from 30 to 50 °C. Dong et al. [4] reported a modal interferometer temperature sensor based on ethanol fully-filled hollow core PCF. The sensitivity is −292 nm/°C with the ethanol-filled PCF 1.9 cm.

Compared with the above types of PCF sensors, PCF sensors based on Sagnac interferometer have been widely used for the measurement of refractive index [5, 6], temperature [7, 8], displacement [9], strain [10] and magnetic field intensity [12] and gas concentration [12] for its high stability, compact structure and easy fabrication. In 1997, Starodumov et al. [13] proposed a Sagnac interferometer-based PCF temperature sensor. The sensitivity was reported to be −0.99 nm/K. Zhang et al. [14] proposed and experimentally demonstrated a temperature sensor based on PANDA fiber Saganac interferometer The sensitivity is up to −1.46 nm/°C as temperature increases from 40 to 50 °C. Cui et al. [15] investigated a temperature sensor based on PCF Sagnac interferometer. The sensitivity is 2.58 nm/°C as fiber length is 11.7 cm and temperature rises from 25 to 42 °C. Shao et al. [16] studied a temperature sensor with cascaded fiber optic Sagnac interferometer based on Vernier-effect. The temperature sensitivity is up from −1.46 nm/°C (single Sagnac configuration) to −13.36 nm/°C (cascaded Sagnac interferometer). Liu et al. [17] proposed a fiber temperature sensor based on fully-filled PCF Sagnac interferometer. High birefringence PCF is produced by increasing the diameter

of the air holes on either side of the core. The average temperature sensitivities is −7.54 nm/°C with temperature from 25 to 85 °C. Shi et al.[18] proposed a temperature sensor based on a fiber ring laser. A Sagnac loop with temperature sensitivity is placed in the resonant cavity of the fiber ring laser. It achieves the temperature sensitivity of 1.739 nm/°C with temperature from 30 to 40 °C.

In this paper, we investigate a temperature sensor based on PCF Sagnac interferometer. The fiber air holes are arranged in hexagonal lattice with uniform arrangement. The two air holes on the left and right sides of the core are removed, so that the PCF has the characteristics of high birefringence. All holes of the PCF are filled with thermal material ethanol. The properties of the temperature sensor are simulated and calculated by the finite element method (FEM) [19–21]. Sensitivities of the temperature sensor are affected by operating wavelength λ and phase birefringence $B(\lambda,T)$. The performances of the temperature sensor with temperature from 45 to 75 °C and 10 to 45 °C are calculated and analyzed. The PCF sensing performances of selective filling and full filling are analyzed and compared with temperature from 45 to 75 °C and fiber length 5.05 cm.

2 Structures of the temperature sensor based on PCF Sagnac interferometer

Figure 1a shows the cross-section of the investigated PCF. The fiber holes in the cladding are arranged in hexagonal lattice with uniform arrangement. The structure parameters are $\Lambda = 3\ \mu m$ and $d = 1.6\ \mu m$. The background material of the PCF is silica and the material dispersion can be expressed by the Sellmeier equation [22]:
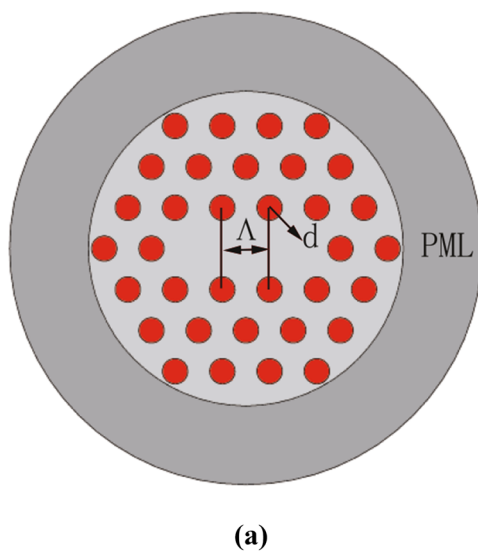
$$n^2 = 1 + \frac{0.6961663\lambda^2}{\lambda^2 - 0.0684043^2} + \frac{0.4079426\lambda^2}{\lambda^2 - 0.1162414^2} + \frac{0.8974794\lambda^2}{\lambda^2 - 9.896161^2},$$

(1)

where λ is the operating wavelength.

All air holes in the cladding are filled with thermal material ethanol and are marked in red [23] as shown in Fig. 1a. The refractive index of ethanol varies with temperature and satisfies the following formula:

$$n = n_0 - \alpha(T - T_0),$$

(2)

where n_0 is the refractive index of ethanol at the temperature of T_0, and α is the thermal coefficient of ethanol. $T_0 = 20$ °C, $n_0 = 1.36048$, $\alpha = 3.94 \times 10^{-4}$ RIU/°C. FEM is used to simulate and calculate the propagation constants of the PCF transmission modes. And the perfectly matched layer (PML) acts as radiation absorber to absorb the radiation energy of the fiber axis. The two holes on either side of the core are removed and the phase birefringence is generated between the formed x and y-polarized core modes. And the electric field distribution of the x and y-polarized core modes is shown in Fig. 1b. The fully-filled PCF with high birefringence can be used for Sagnac interferometric sensing.

Figure 2 illustrates the schematic diagram of the PCF temperature sensor based on Sagnac interferometer. The orange line and gray line represent the high birefringence PCF and single-mode fiber (SMF), respectively. PCF sensor based on Sagnac interferometer consists of PCF fused with SMF, 3 dB optical coupler (OC), polarization controller (PC), broadband source (BBS) and optical spectrum analyzer (OSA). We use the welding machine to fuse the PCF with SMF. The PCF fully filled with ethanol is placed in a constant-temperature bath. The light emitted by the BBS is divided into two identical
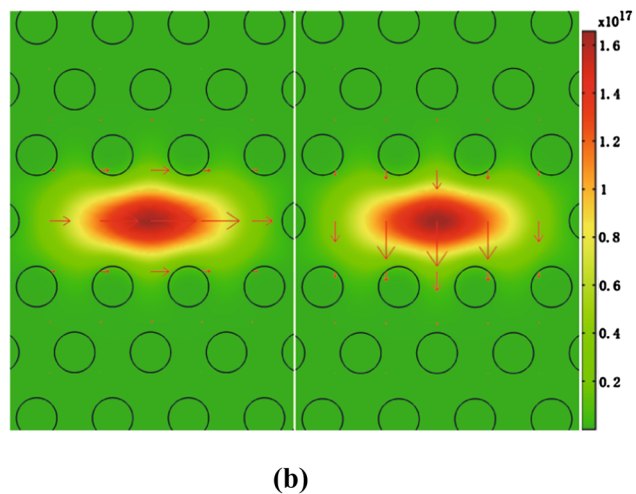

(a)   (b)

Fig. 1 **a** Cross-section of the PCF fully filled with ethanol. **b** The electric field distribution of x and y-polarized core modes
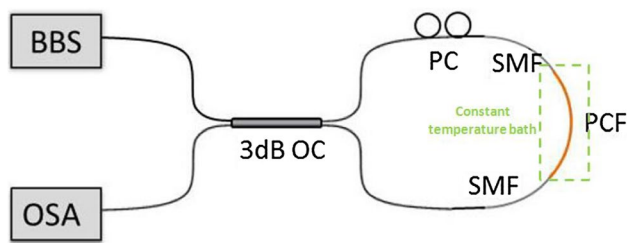
Fig. 2 The schematic diagram of the temperature sensor based on Sagnac interferometer

(a)

(b)

Fig. 3 **a** Phase birefringence dependence on temperature. **b** Phase birefringence B and group birefringence B$_g$ versus with wavelength, $T = 60\,°C$

beams by 3 dB OC and transmitted in the opposite direction in the optical path. The combination of the PC and the high birefringence PCF causes the phase difference between the same polarization states of the two beams transmitted to 3dB OC. The generation of phase difference satisfies interference conditions and interference occurs. The transmission curves can be detected by OSA. The transmission spectrum will shift with the the change of temperature.

The transmission spectrum of the PCF temperature sensor based on Sagnac interferometer can be expressed as[24]:

$$T = \frac{1 - \cos \varphi}{2} = \frac{1 - \cos\left(\frac{2\pi BL}{\lambda}\right)}{2}, \tag{3}$$

where φ is the phase difference, n_x and n_y are the effective refractive index of the x and y polarization modes, $B = (n_x - n_y)$ is the phase birefringence, and L represents the length of the PCF filled with ethanol.

When $\varphi = 2m\pi$, T takes the maximum and the corresponding wavelength is the dip wavelength. That is:

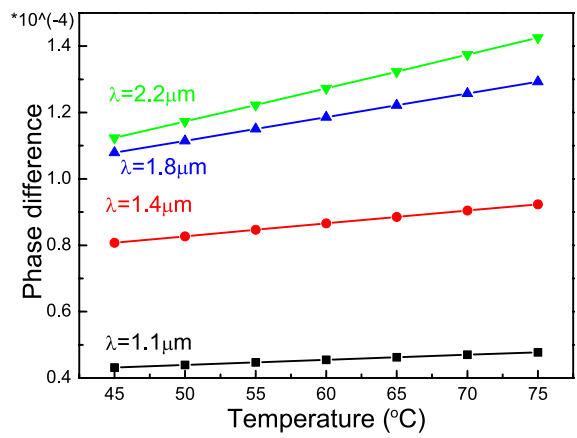$$\varphi = \frac{2\pi BL}{\lambda} = 2m\pi, \tag{4}$$

where m is integer. The parameters $B(\lambda,T)$, λ, L are temperature dependent. The upper formula derivatives of T can be obtained:

$$\frac{\left[L\frac{\partial B(\lambda,T)}{\partial T} + L\frac{\partial B(\lambda,T)}{\partial \lambda}\frac{d\lambda(T)}{dT} + B(\lambda,T)\frac{dL}{dT}\right]\lambda(T)}{\lambda^2(T)} - \frac{B(\lambda,T)L\frac{dL}{dT}}{\lambda^2(T)} = 0. \tag{5}$$
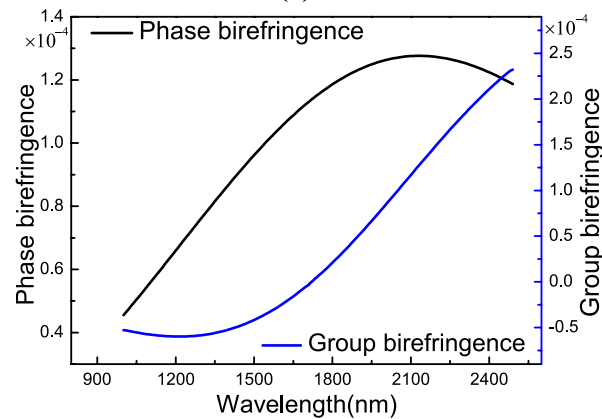
The temperature sensitivity $S(\lambda,T)$ is the change of the dip wavelength λ divided by the change of the corresponding temperature T:

$$S(\lambda,T) = \frac{d\lambda}{dT} = \frac{\frac{\partial B(\lambda,T)}{\partial T}\lambda(T)}{B_g(\lambda,T)}, \tag{6}$$

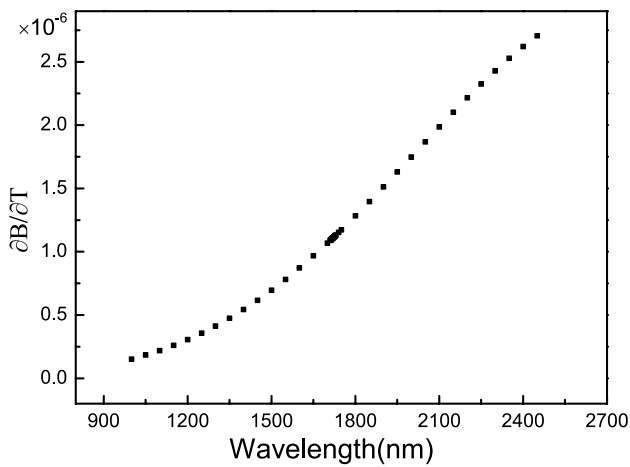where the group birefringence $B_g = B(\lambda,T) - \lambda\frac{dB(\lambda,T)}{d\lambda}$.
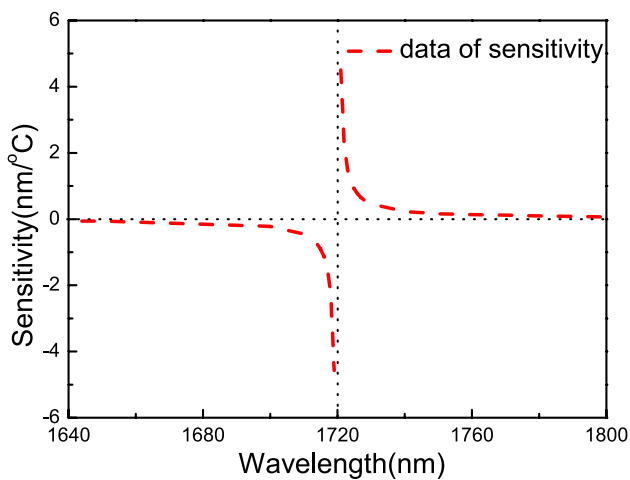
3 Results and discussion

The phase birefringence dependence on temperature at different wavelength is shown in Fig. 3a. The effective refractive index of the x polarization is larger than that of the y polarization, so the phase birefringence B is positive. The phase birefringence increases as the refractive index of the ethanol decreases with the increase of the temperature. Figure 3b shows the phase birefringence B and the group birefringence B_g versus wavelength at 60 °C. As wavelength increases from 0.9 to 2.5 µm, the phase birefringence increases first and then decreases with the increase of the wavelength and the change law of B$_g$ is contrary to B. When the operating wavelength is less than 1720 nm, group birefringence is negative and when the operating wavelength is greater than 1720 nm, the group birefringence is positive. According to Fig. 3, phase birefringence B is related to temperature and operating wavelength. The sensitivity of B with temperature at different wavelength can be obtained

by linear fitting ($S(B,T) = \partial B/\partial T$), as shown in Fig. 4a. $\partial B/\partial T$ increases with the increase of wavelength and is positive.

The parameters B, B_g and $\partial B/\partial T$ in formula (6) are analyzed and calculated. Their relationship with wavelength is shown in Figs. 3 and 4a. The above parameters are brought into formula (6). The relationship curve of sensitivity with wavelength is obtained, as shown in Fig. 4b. According to the formula (6), the sensitivity is negatively correlated with group birefringence B_g and positively correlated with $\partial B/\partial T$ and λ. The group birefringence B_g is negative first and then positive, and 1720 nm is the dividing line. λ, B and $\partial B/\partial T$ are positive. The sign of sensitivity is related to group birefringence B_g. When the wavelength is less than 1720 nm, the sensitivity is negative and increases with the increase of the wavelength. The sensitivity is positive and decreases as the wavelength increases from 1720 nm. The temperature sensitivity is rapidly declining near 1720 nm.

When we set the fiber length 5.05 cm, the transmission curves of the temperature sensor with temperature from 45 to 75 °C are shown in Fig. 5a. The two dip wavelengths move in the opposite direction with the increase of temperature. The wavelength of dip 1 experiences a blue-shift and the dip wavelength varies from 1.5 to 1.23 µm. The wavelength of the dip 2 experiences a red-shift with the increase of the temperature and the dip wavelength changes from 1.846 to 2.361 µm. Figure 5b shows the dip wavelengths versus temperature and gives the numerical fitting results. For dip 1 and dip 2, the corresponding sensitivities are −8.7657 and 16.8142 nm/°C. And the corresponding R-squares are 0.9467 and 0.98613. If the resolution of the OSA is 0.01 nm, the resolutions of the PCF temperature sensor are 0.00114 and 0.00059 °C, respectively.

Fig. 4 a $\partial B/\partial T$ versus with wavelength. **b** Sensitivity of temperature sensor dependence on wavelength
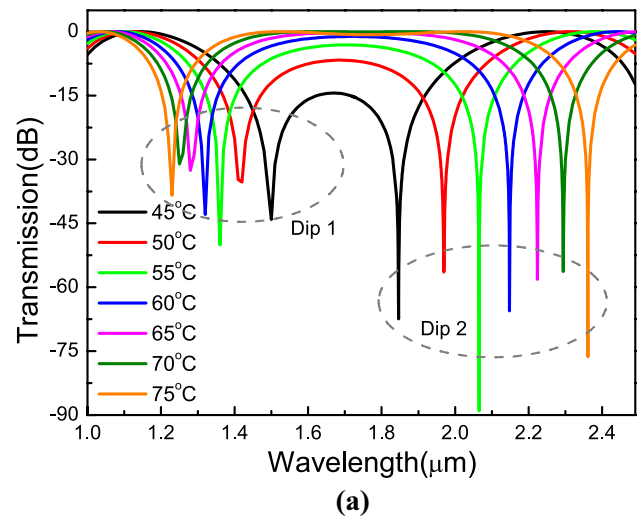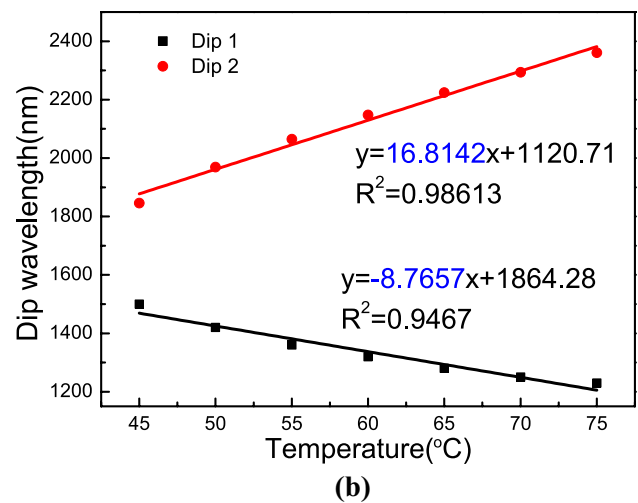
Fig. 5 a $L = 5.05$ cm, Transmission curves of the PCF dependence on the wavelength with temperature varying from 45 to 75 °C. **b** Two dip wavelengths versus temperature. Sensitivities of the temperature sensor are −8.7657 and 16.8124 nm/°C

According to the formula 6, the variation of B, B_g and $\frac{\partial B}{\partial T}$ with wavelength does not change with the fiber length L. The wavelength where the sensitivity is converted from negative to positive is 1600 nm at the temperature of 25 °C. When we set $L = 2.11$ cm, the transmission curves of the PCF are illustrated in Fig. 6a as temperature changes from 10 to 45 °C. The dip 1 and dip 2 experience a blue-shift and red-shift with the increase of the temperature, respectively. Dip 1 moves from 1.38 to 1.092 µm and dip 2 moves from 1.714 to 2.312 µm with the increase of the temperature. Figure 6b shows the dip wavelength varying with temperature and gives the fitting results. The sensitivities of dip 1 and dip 2 are −7.848 and 16.655 nm/°C and the corresponding adjusted R-square are 0.9406 and 0.9861, respectively. If

(a)

(b)

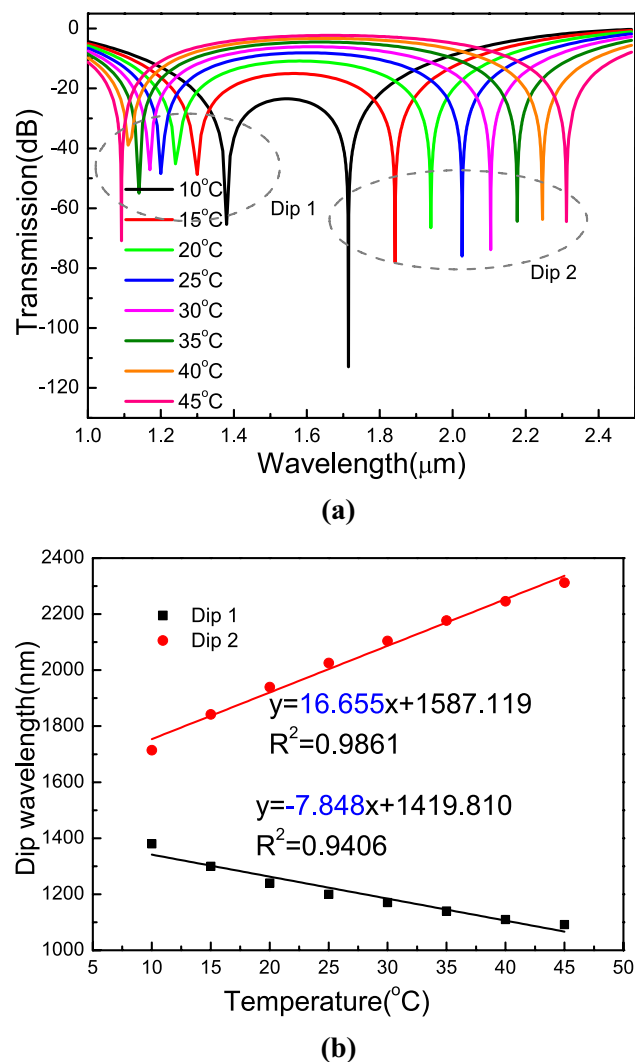**Fig. 6** **a** $L = 2.11$ cm, Transmission curves of the sensor relying on the wavelength with temperature varying from 10 to 45 °C. **b** Two dip wavelengths versus temperature. Sensitivities are −7.848 and 16.655 nm/°C

the resolution of the OSA is 0.01 nm, the resolutions of the temperature sensor are 0.00127 and 0.0006 °C.

Figure 7 gives three types of the cross-section of the PCF filled with different air holes. Figure 8 is the transmission and sensitivity curves corresponding to the three cross-sections of Fig. 7 with fiber length $L = 5.05$ cm. As shown in Fig. 7a, the air holes on either side of the core are selectively filled with ethanol. The final transmission curves are shown in Fig. 8a. The sensitivity of the dip wavelength near 1445 nm is calculated and the linear fitting result is shown in Fig. 7d. The sensitivity is only 0.12143 nm/°C with poor linearity.

Figure 7b shows that the four air holes up and down the core are selectively filled with ethanol. The transmission spectra are shown in Fig. 8b. There are three dips in the allowable wavelength range of the silica PCF. We choose the first dip for temperature sensing measurement with temperature from 45 to 75 °C. Figure 8e is the sensitivity linear fitting. The sensitivity is −4.843 nm/°C with the adjusted R-square of 0.9906. Figure 7c is the cross-section of the PCF with the first layer of the cladding selectively filled. Figure 8c shows the corresponding transmission curve with $L = 5.05$ cm. There are two dip wavelengths moving to short wavelength with the increase of temperature. The dip wavelengths experience blue-shift. The sensitivity of the temperature sensor is −4.621 and −14.593 nm/°C. The corresponding adjusted R-square are 0.994 and 0.9852, respectively.

Compared with the performance of the above three cross-section of the PCF filled with different air holes, the fully-filled PCF has the following advantages: low filling difficulty and technical requirement, wide temperature range and higher temperature sensitivities.

Figure 9a illustrates the cross-section of the fully-filled PCF that the air holes in the left and right of the core are not moved. Fig. 9b, c illustrates the electric filed distribution of x- and y-polarized core modes. This structure PCF cannot produce birefringence, so this kind of structure PCF cannot be used for Sagnac interferometric temperature sensing.

Table 1 lists sensing data of various temperature sensors and compared with temperature sensor based on fully ethanol-filled PCF Sagnac interferometer in this paper.

4 Conclusions

A temperature sensor based on PCF Sagnac interferometer is investigated with all fiber holes filled with ethanol. The sign of sensitivity is determined by group birefringence B_g and changes at the zero-point wavelength. The transmission curves show that the two dip wavelengths shift in opposite direction with the temperature from 10 to 75 °C. The temperature sensitivities can reach −8.7657 and 16.8142 nm/°C with fiber length 5.05 cm and temperature

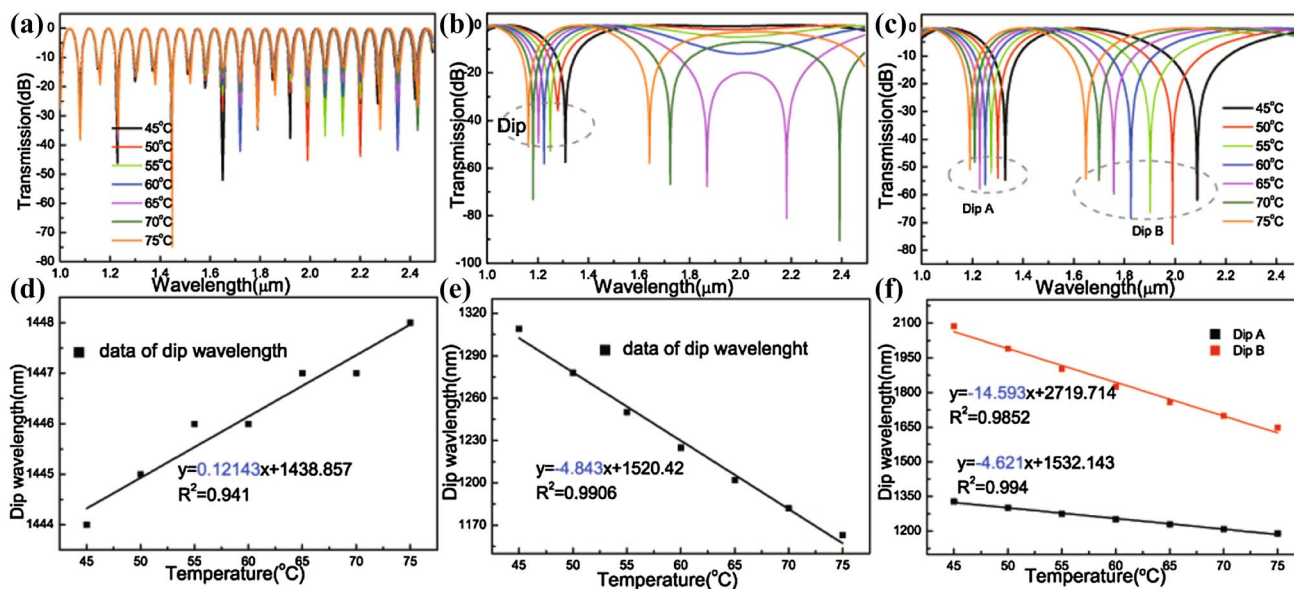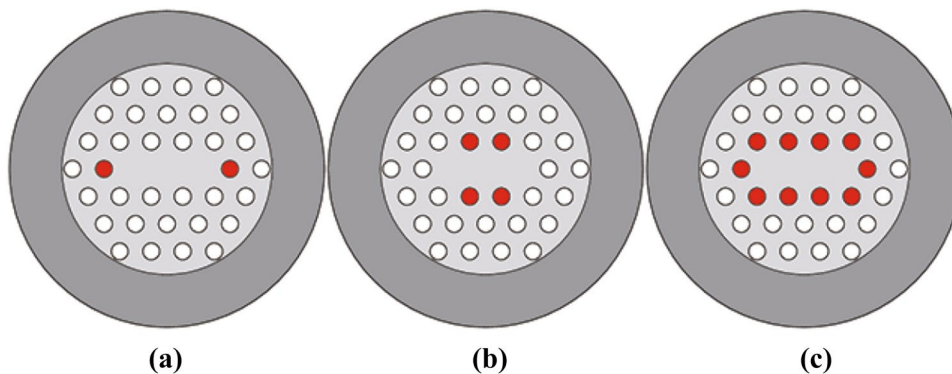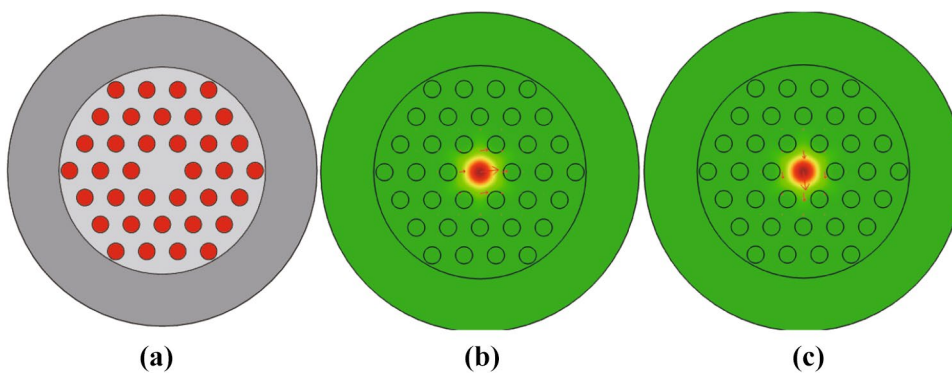**Fig. 7** Three types of cross-section of the PCF with different air holes filled

Fig. 8 Transmission curves and the sensitivity fitting results of the dip wavelength of the three different selectively filling PCF

Fig. 9 Cross-section and core modes of the PCF with the air holes arranged in hexagonal lattice

from 45 to 75 °C. The temperature sensitivities can be up to -7.848 and 16.655 nm/°C with $L = 2.11$ cm and temperature from 10 to 45 °C. Compared with selective filling, full filled PCF can better achieve the effect of high birefringence and temperature sensing with temperature from 45 to 75 °C and $L = 5.05$ cm. Considering its simple

structure and high sensitivities, the temperature sensor has high application value for temperature detection.

Table 1 Comparison of sensing data of various temperature sensors

Type	Sensitivity (nm/°C)	Detecting window (°C)
Surface plasmon resonance	10	30–50 [3]
Mode coupling	−1.85, −1.95	20–80 [25]
Mach–Zehnder	−1.83, −1.09	23.2–28.5 [2]
Sagnac	2.58	25–42 [15]
Sagnac, Vernier-effect	−13.36	30–40 [16]
This paper	−8.7657, 16.8124	45–75
	−7.848, 16.655	10–45

References

1. P. Russell, J. Lightwave Technol. **299**, 358 (2003)
2. Y. Geng, X. Li, X. Tan, Y. Deng, IEEE Sens. J. **14**(1), 167–170 (2014)
3. M.F.O. Hameed, M.Y. Azab, A.M. Heikal, S.M. El-Hefnawy, S.S.A. Obayya, IEEE Photonics Technol. Lett. **28**(1), 59–62 (2015)
4. B. Dong, C.Y. Yu , Y.X. Wang, International Conference on Optical Communications and Networks, 1–3 (2015)
5. P. Gao, X. Chen, W. Feng, Rev. Sci. Instrum. **83**(10), 1752–1757 (2012)
6. P. Zu, C.C. Chan, W.K. Guo, S.L. Wen, Y. Jin, H.F. Liew, C.W. Wei, X. Dong, Sens. Actuators B Chem. **191**(2), 19–23 (2014)
7. C. Zhong, C.L. Zhao, H.F. Wei, J.T. Guo, L. Qi, S.Z. Jin, S.Q. Zhang, Z.X. Zhang, Z.Q. Wang, Opt. Lett. **37**(22), 4789 (2012)
8. T. Han, Y. Liu, Z. Wang, J. Guo, Z. Wu, S. Wang, Z. Li, W. Zhou, Opt. Express **21**(1), 122–8 (2013)
9. A.M.R. Pinto, J. Kobelke, K. Schuster, M. Bravo, M. Lopez-Amo, Opt. Lett. **37**(2), 202–4 (2012)
10. X.Y. Dong, H.Y. Tam, P. Shum, Appl. Phys. Lett. **90**(15), 1099–1102 (2007)
11. Q. Liu, S.G. Li, X. Wang, Sens. Actuators B Chem. **242**, 949–955 (2016)
12. H.W. Zhang, L.C. Duan, W. Shi, Q. Sheng, Y. Lu, J.Q. Yao, Sens. Actuators B Chem. **247**, 124–128 (2017)
13. A.N. Starodumov, L.A. Zenteno, D. Monzon, E. De La Rosa, Appl. Phys. Lett. **70**(1), 19–21 (1997)
14. J. Zhang, X. Qiao, T. Guo, Y. Weng, R. Wang, Y. Ma, Q. Rong, M. Hu, Z. Feng, J. Lightwave Technol. **29**(24), 3640–3644 (2011)
15. Y. Cui, P.P. Shum, D.J.J. Hu, G. Wang, G. Humbert, X.Q. Dinh, IEEE Photonics J. **4**(5), 1801–1808 (2012)
16. L.Y. Shao, Y. Luo, Z. Zhang, X. Zou, B. Luo, W. Pan, L. Yan, Opt. Commun. **336**, 73–76 (2015)
17. Q. Liu, S.G. Li, M. Shi, Opt. Commun. **381**, 1 (2016)
18. J. Shi, Y.Y. Wang, D.G. Xu, H.W. Zhang, G.H. Su, L.C. Duan, C. Yan, D.X. Yan, S.J. Fu, J.Q. Yao, IEEE Photonic Tech. L. **28**(7), 794–797 (2016)
19. A.A.A. Pradhan, C. Siau, A. Constantin, P.B.S. Clarke, IEICE Trans. Inf. Syst. E **85C**(4), 881–888 (2002)
20. K. Saitoh, M. Koshiba, IEEE J. Quantum Electron. **38**(7), 927–933 (2002)
21. Y.J. He, Sens. Actuators B Chem. **183**(13), 319–331 (2013)
22. G. Ghosh, M. Endo, T. Iwasaki, J. Lightwave Technol. **12**(8), 1338–1342 (1994)
23. K. Nielsen, D. Noordegraaf, T. Sørensen, A. Bjarklev, T.P. Hansen, J. Opt. A Pure Appl. Opt. **7**, L13 (2005)
24. T. Han, Y.G. Liu, Z. Wang, J. Guo, Z. Wu, M. Luo, S. Li, J. Wang, W. Wang, Opt. Express **22**(12), 15002–16 (2014)
25. Q. Liu, S.G. Li, H.L Chen, Z.K. Fan, J.S. Li, IEEE Photonics J. **7**(2), 1–9 (2015)